ISSN 0021-3640, JETP Letters, 2019, Vol. 110, No. 3, pp. 223–230. © Pleiades Publishing, Inc., 2019.
Russian Text © The Author(s), 2019, published in Pis'ma v Zhurnal Eksperimental'noi i Teoreticheskoi Fiziki, 2019, Vol. 110, No. 3, pp. 204–212.

CONDENSED MATTER

Effect of a Substrate on the Magnetoelectric Effect in Rare-Earth-Doped Bismuth Iron Garnet

S. S. Aplesnin[a, b, *], A. N. Masyugin[a], M. N. Sitnikov[a], and T. Ishibashi[c]

[a] *Reshetnev Siberian State University of Science and Technology, Krasnoyarsk, 660014 Russia*

[b] *Kirensky Institute of Physics, Federal Research Center KSC, Siberian Branch, Russian Academy of Sciences, Krasnoyarsk, 660036 Russia*

[c] *Department of Materials Science and Technology, Nagaoka University of Technology, Nagaoka, Niigata, 940-2188 Japan*

**e-mail: apl@iph.krasn.ru*

Received June 17, 2019; revised July 4, 2019; accepted July 4, 2019

The mechanism of relaxation of the electric polarization in thin films of rare-earth-doped bismuth iron garnet on glass and gallium gadolinium garnet substrates is determined in magnetic fields of 0 and 12 kOe in the temperature range of 80–380 K. The change in the sign of the residual electric polarization after switching off the electric field and the magnetic-field-induced shift of the hysteresis loop in the applied magnetic field are found. Linear and quadratic magnetoelectric effects with the tensor components depending on the substrate type are observed. The linear magnetoelectric effect is related to the spin–orbit coupling of electrons at the film–substrate interface, whereas the quadratic one is determined by the exchange–striction mechanism.

DOI: 10.1134/S0021364019150074

1. INTRODUCTION

Bismuth iron garnets exhibit colossal Faraday rotation in the visible spectral range and are used in magneto-optical devices for the spatial modulation of light and in optical sensors [1–3]. Yttrium iron garnet is characterized by cubic symmetry with an inversion center. At low temperatures (below 130 K), it exhibits the structural transition accompanied by the triclinic lattice distortion and the linear magnetoelectric (ME) effect [4]. Bulk rare earth iron garnets exhibit the quadratic ME effect [5].

For spintronic devices, it is important to control magnetic characteristics by the applied electric field. In the garnet-ferrite films, the possibility of local nucleation of bubble domains by applying an electrically charged probe to a single-domain state was demonstrated in experiment [6]. In multiferroics, the electric field can induce topologically protected magnetic defects such as skyrmions. This occurs since magnetic domain walls effectively acquire a negative surface energy [7]. In 10-μm-thick $(BiLu)_3(FeGa)_5O_{12}$ films grown by liquid-phase epitaxy at the $Gd_3Ga_5O_{12}$ substrate oriented in the (210) direction, the electric-field-induced motion of domain walls was observed [8] and change in their electric polarization was detected [9]. Such change is not observed in the films deposited on the (111) oriented substrate. These effects are interpreted in terms of the inhomogeneous magnetoelectric coupling and the electric-field-induced change in magnetic anisotropy [10–12]. The latter factor can be excluded for the measurements performed in the applied magnetic field exceeding by an order of magnitude its saturation value. An anomalously large linear ME effect is observed in epitaxial iron garnet films in the magnetic field up to 5 kOe [13]. This effect is usually related to the nonuniform substrate-induced deformations of the film. In 90-nm-thick $Bi_3Fe_5O_{12}$ (BIG) films, the ferromagnetic resonance technique with the electric field modulation reveals the linear ME effect with the peak at 450 K. Such effect is due to the strong spin–orbit coupling and to the formation of local magnetic inhomogeneities and is directly related to bismuth ions [14]. The linear ME effect is detected in the films through electric-field-induced change in the magnetization. The electric polarization of the films in the applied magnetic field has not yet been studied. The contribution to the ME effect from EH and EH^2 is still not clear.

The electric polarization can be due to the structural distortion breaking the inversion center symmetry. This distortion is caused by stresses generated by the epitaxial film growth at the substrate or by the cation substitution at dodecahedral sites. The polarization can also result from the surface electron states, magnetic domain structure induced by stray fields, and spin–orbit coupling.

The electron density functional calculation of the electronic structure of BIG taking into account rela-

tivistic corrections demonstrates the enhancement of spin–orbit coupling owing to the hybridization of 6*p* orbitals of bismuth with the electronic states of oxygen and iron [15]. Experimentally determined spin–orbit splittings of t_{2g} states of iron ions are equal to 39.4 meV [16]. The nuclear magnetic resonance study demonstrated that bismuth ions in $Bi_3Fe_5O_{12}$ have a magnetic moment of 0.1 μ_B/atom caused by the hyperfine interaction and the *s*–*p* hybridization of Bi–O orbitals [17]. At nonzero applied magnetic field, the change in the splitting of p_α ($\alpha = x, y, z$) orbitals leads to the shift of the electron density at the Bi–O bond and to the local electric polarization. At the film–substrate interface, the formation of topological states described by the Rashba model [18] is possible. The splitting of spin-up and spin-down subbands in the magnetic field also leads to the change in the electron density of states at the level of the chemical potential and gives rise to the electric polarization. In this case, the tensor describing the ME coupling depends on the phase of the electron wavefunction, which can be controlled by the applied magnetic field [19, 20]. An indirect confirmation of a nonzero orbital angular momentum is the anisotropy of saturation magnetization in $Nd_2Bi_1Fe_4Ga_1O_{12}$ films at room temperature [21].

The quadratic ME effect in the magnetic field results from the exchange–striction mechanism. The bismuth-substituted neodymium–iron garnet films exhibit the peak and the sign change in the temperature dependence of magnetostriction [22].

The work is aimed at finding the electric polarization and determining the mechanism of ME coupling in neodymium–bismuth iron garnet films deposited on garnet and glass substrates in a high magnetic field.

2. RELAXATION OF THE ELECTRIC POLARIZATION AND THE ELECTRIC FIELD DEPENDENCE OF THE POLARIZATION

We studied epitaxial $Nd_1Bi_2Fe_5O_{12}$(450 nm)/$Nd_2Bi_1Fe_4Ga_1O_{12}$(90 nm) films on the glass substrate and $Nd_{0.5}Bi_{2.5}Fe_5O_{12}$(450 nm) films on the monocrystalline gadolinium gallium garnet (GGG) substrate grown along the (111) direction. The films were prepared by the decomposition of metalorganic compounds extracted from the solution [23]. The previous X-ray structural analysis did not reveal the peaks corresponding to the polycrystalline material [21]. Magnetic hysteresis loops were measured at magnetic fields up to 2 kOe applied perpendicular to the film surface. The magnetization saturation field is 0.5 kOe, whereas the saturation magnetization in the film plane is 15% higher than that normal to the film [21].

The electric polarization in the film plane is determined by measuring the electric charge using a Keithley 6517B electrometer by switching on and off the dc electric field applied along the film (Fig. 1a).

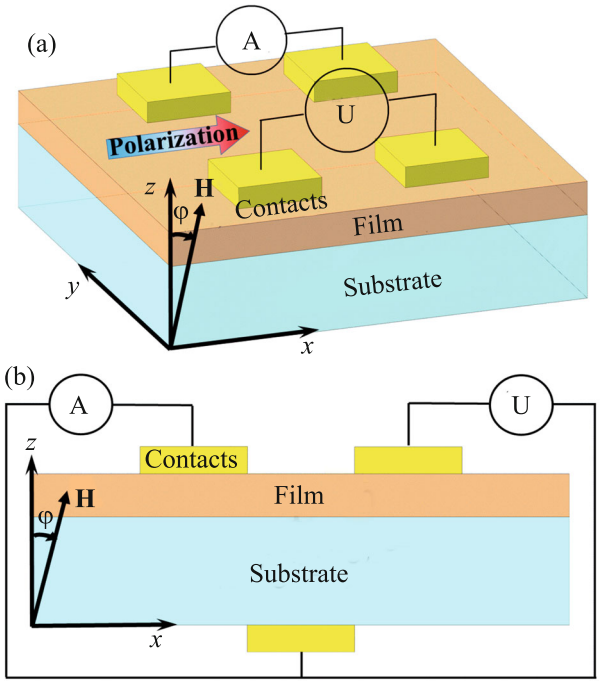

Fig. 1. (Color online) Schematic of the measurement of the electric polarization (a) parallel and (b) perpendicular to the film at different strengths and directions of the applied magnetic field.

The formation of disclinations, elastic stresses, and band bending is possible near the film–substrate interface, which can lead to the migration-induced electric polarization. Another possible mechanism of the enhancement of the electric polarization is related to the electron density redistribution for the hybridized *s*–*p* orbitals of bismuth ions. The relaxation time corresponding to the migration-induced polarization is 0.1–10^3 s and it is observed in a dc electric field or at rather low frequencies of the driving electromagnetic field.

The relaxation time is found using the time dependence of the electric polarization at switching on and off the applied electric field with a strength of 600 V/cm and different orientations at a frequency of 0.01 Hz. In Fig. 2a, we show the relative change in the electric polarization of the film deposited on the garnet substrate after switching on the dc electric field. Below 280 K, the electric polarization increases in the applied electric field according to the exponential law $\Delta P/P = \exp(t/\tau)$, and it is described by the Debye model. The relaxation time of the electric polarization decreases on heating from $\tau = 170$ s at $T = 80$ K to $\tau = 140$ s at $T = 200$ K. At $T = 280$ K, the relaxation time of the electric polarization changes its behavior from an exponential to a power law $\Delta P/P = (t/\tau)^\alpha$, where $\alpha \approx 1.25$ and the relaxation time itself decreases from $\tau = 30$ s to $\tau = 5$ s at $T = 360$ K. The relaxation

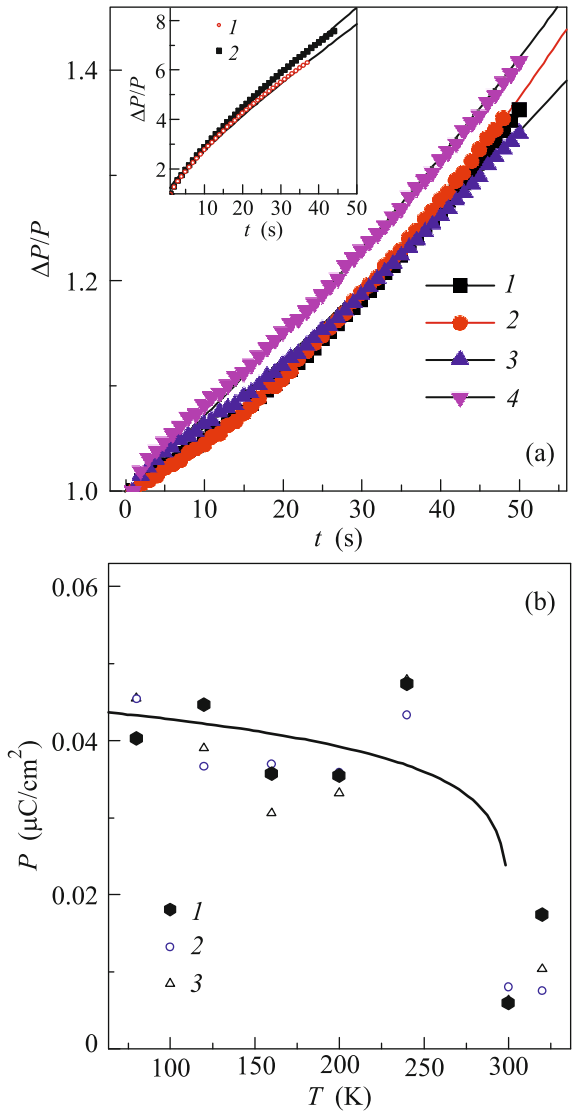

Fig. 2. (Color online) (a) Time dependence of the relative change in the electric polarization along the film deposited on the garnet substrate after switching on the dc electric field $E = 600$ V/cm at temperatures $T = (1)$ 80, (2) 120, (3) 160, and (4) 200 K. The inset illustrates the behavior of $\Delta P/P$ at $T = 360$ K for (1) $H = 0$ and (2) $H^z = 12$ kOe. (b) Temperature dependence of the residual polarization at $t =$ 200 s in magnetic fields (1) $H = 0$, (2) $H^z = 12$ kOe, and (3) $H^x = 12$ kOe.

time of the electric polarization increases in the applied magnetic field. After switching off the electric field, the sign of the residual electric polarization does not change. In Fig. 2b, we illustrate the behavior of the residual electric polarization at 50 s after switching off the electric field in the absence and presence of the magnetic field with different orientations with respect to the film. The anisotropy of the residual electric polarization in the applied magnetic field is observed at the rotation of the polarization by $\pi/2$. Another possible mechanism of the increase in the electric polarization is due to the electron density redistribution in the hybridized s–p orbitals of bismuth ions. In the case of migration-induced polarization, the relaxation time is $0.1–10^3$ s. It is observed in the applied dc electric field or at quite low frequencies of the driving electromagnetic field.

The relaxation time of the electric polarization can be found from its time dependence at switching on and off the electric field normal to the film with a strength of 600 V/cm. The residual electric polarization decreases by several times on heating up to room temperature (Fig. 2b).

For the film deposited on the glass substrate, the electric polarization changes its sign after switching off the electric field (Fig. 3a). After switching on the electric field, the electric polarization obeys the power law $\Delta P/P = A(t)^{\alpha}$ with the exponent $\alpha \approx 0.6$ in the temperature range of 80–280 K. The electric polarizations in the magnetic fields perpendicular and parallel to the film are different. In Fig. 3b, we show the residual electric polarization at $t = 200$ s. Below 200 K, the residual electric polarization decreases in the magnetic field, whereas above 200 K, the components of the ME tensor have different signs.

The electric polarization $P(E, H)$ as a function of the electric and magnetic fields is determined along the normal to the film (Fig. 1b) using the relation $P = \int jdt$, where the electric current is measured in the quasiperiodic electric field with the frequency $\nu = 0.01$ Hz at different orientations of the magnetic field. Hysteresis is observed at high electric fields (Fig. 4) and is related to the formation of quasidegenerate states in potential wells at the substrate–film interface. On heating, the width of the $P(E)$ hysteresis loops in the magnetic field achieves its maximum at $T = 240$ K.

The electric field dependence of the electric polarization for the film deposited on the glass substrate exhibits a hysteresis (Fig. 5), which becomes shifted under effect of the applied magnetic field along the polarization axis. The width of the $P(E)$ hysteresis loop depends on the magnetic field direction with respect to the film and does not exceed 0.15 μC/cm^2. The electric polarization for the films deposited on the glass substrate is 30–60% larger than that for the films on the garnet substrate.

3. MAGNETOELECTRIC EFFECT

In the magnetic field dependence of the electric polarization, we retain only the terms up to the second order: $P_i = \varepsilon_{ij}\varepsilon_0 E_j + \alpha_{ij}H_j + \gamma_{ijk}H_jH_k + \beta_{ijk}E_jH_k$. In Fig. 6, we plot $P(H)$ for the film deposited on the garnet substrate in the temperature range of 80–360 K. At all temperatures, we observe a monotonic magnetic

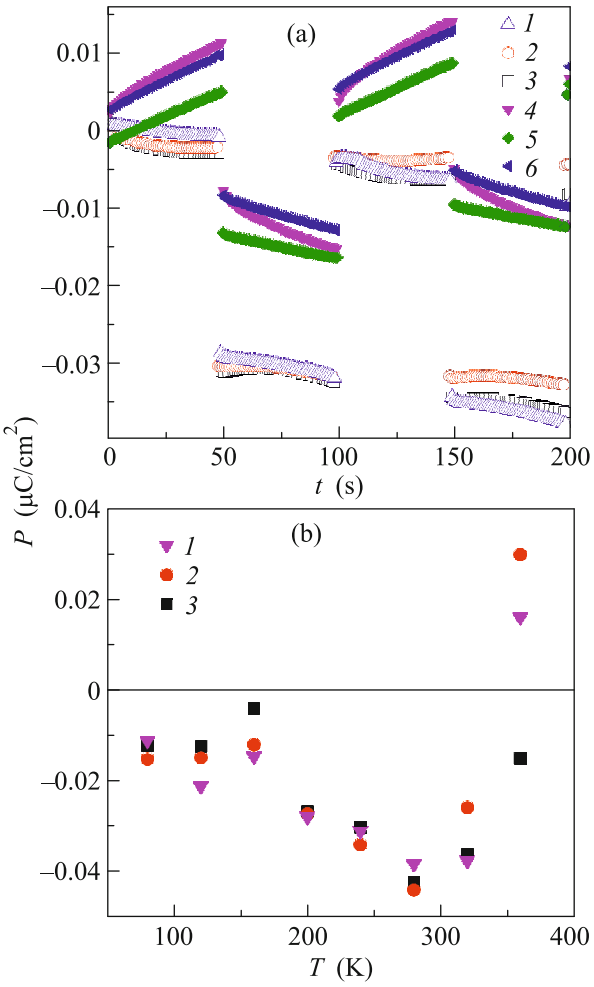

Fig. 3. (Color online) (a) Electric polarization along the film deposited on the glass substrate after switching on and off electric field $E = 600$ V/cm with a frequency of 0.01 Hz at T = (*1–3*) 320 and (*4–6*) 80 K in magnetic fields $H = 0$ (*1*, *4*), $H^z = 12$ kOe (*2*, *6*), and $H^x = 12$ kOe (*3*, *5*). (b) Temperature dependence of the residual polarization at $t = 200$ s in magnetic fields (*1*) $H = 0$, (*2*) $H^z = 12$ kOe, and (*3*) $H^x = 12$ kOe.

field dependence of the electric polarization. The magnetoelectric coupling is due to the spin–orbit interaction with the linear field dependence and to the magnetoelectric interaction with the quadratic field dependence; thus, we have $P_i(H) = \alpha_{ij}H_j + \gamma_{ij}H_j^2$.

At $T = 80$ K, the induced electric polarization is an even function of the magnetic field normal, $P(H^z)$, and parallel, $P(H^x)$, to the film. On heating up to $T = 120$ K, the polarization $P(H^z)$ changes its sign, whereas $P(H^x)$ remains positive at the reversal of the magnetic field (Fig. 6a). At $T = 160$ K, the sign of $P(H^z)$ changes at the reversal of the magnetic field direction, $H \to -H$, and the polarization at the magnetic field along the film achieves the maximum value. The polarizations $P(H^x)$ and $P(-H^x)$ are positive and differ by two orders of magnitude from $P(-H^z)$ at $T = 200$ K. At $T = 240$ K, the diagonal components of the linear and quadratic ME tensors are comparable, whereas $P(-H^z)$ is an order of magnitude larger than $P(H^z)$ (Fig. 6b). Near room temperature, the linear ME effect is dominant for the longitudinal component of the tensor α_{ij} and quadratic one prevails in the off-diagonal γ_{ij} components (Fig. 6c). At $T = 360$ K, the signs of the polarization depend on the magnetic field direction (Fig. 6d).

For the film deposited on the glass substrate, the linear contribution to the ME coupling prevails (Fig. 7) and achieves the maximum value at $T = 200$ K. The sign of the polarization does not change at the reversal of the magnetic field normal to the film, and the quadratic contribution to the ME coupling is dominant above 280 K (Fig. 7d).

4. MODEL

At the interface between the magnetic medium and insulator, the space inversion and time reversal symmetries are broken: the symmetry center is absent in the near-interface layers, whereas the magnetic ordering in one of the adjacent materials breaks the time reversal symmetry. Thus, the interface favors the conditions for the ME effect [24]. It is possible to distinguish three main mechanisms of the magnetically induced electric polarization in multiferroics: (a) polar ionic displacements changing the bond angles between magnetic ions and ligands and affecting the exchange field and relative orientations of magnetic moments [25], (b) the interplay between the spatial spin modulation and the electric polarization due to the relativistic mechanism [26], and (c) the electron density redistribution caused by the spin–orbit coupling [27, 28].

Bismuth ions with the hybridization of s and p states and impurity Fe^{2+} ions having a nonzero orbital magnetic moment make a linear contribution in magnetic field to the ME effect. The polarizability of cations $\alpha_n \sim (M_J^2 - 1/3J(J+1))$ depends on the projection of the total magnetic moment on the specified axis. The magnetic field lifts degeneracy with respect to the magnetic moment and leads to an increase in the polarizability and to the electric polarization. Another issue is related to the band orbital angular momentum of an electron in the magnetic field, described by the Hamiltonian [20]

$$H = \sum_i E_i n_i + \sum_{ij} t_{ij} e^{i\varphi} C_i^+ C_j^-, \qquad (1)$$

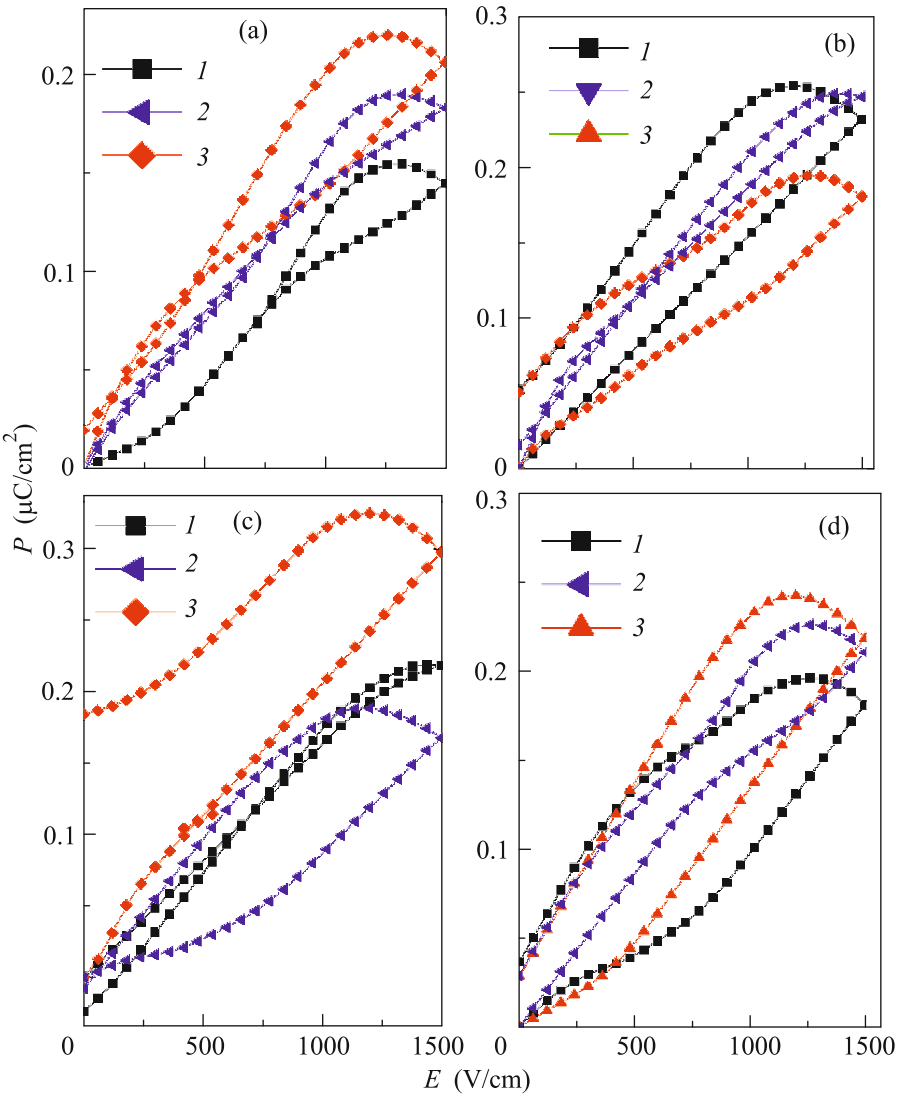

Fig. 4. (Color online) Electric polarization normal to the film deposited on the GGG substrate versus the applied electric field (*1*) at zero magnetic field $H = 0$, (*2*) at the magnetic field $H^z = 12$ kOe normal to the film, and (*3*) at the magnetic field $H^x = 12$ kOe along the film at temperatures $T =$ (a) 80, (b) 160, (c) 240, and (d) 320 K.

where E_i is the electron energy in the band with the occupation number n_i, t is the hopping integral, and φ is the phase of the electron wavefunction, which depends on the magnetic field and on the number of bands [20]. The components of the linear ME effect, whose signs and magnitudes depend on the phase of the electron wavefunction varying in the range of 0–2π, are calculated numerically. The sign of the tensor components at the fixed phase depends on the number of electron bands and changes from negative to positive [20]. The magnetic-field-induced narrowing of the impurity subband for the film deposited on the garnet substrate leads to an increase in the effective mass of charge carriers, to a decrease in their mobility, and to an increase in the phase. This increases the magnitude of the ME tensor.

The simultaneous action of the spin–orbit coupling, odd part of the crystal field potential, and applied electric field changes the magnetic anisotropy field and leads to the EH^2 ME effect with respect to the electric field. The quadratic ME effect related to the anisotropic Dzyaloshinskii–Moriya exchange ($D[\mathbf{S}_1 \times \mathbf{S}_2]$) and to the indirect exchange interaction $J\mathbf{S}_1\mathbf{S}_2$ resulting from the displacements of ligand ions can be described by the expression [29]

$$H_{\text{me}} = \sum_k \sum_{ij} \beta_1 S_i^z u_k S_j^z + \beta_2 S_i^x u_k S_j^y, \qquad (2)$$

where $\beta_1 = dJ/du$ and $\beta_2 = dD/du$ are the strain-induced changes in the bilinear and antisymmetric

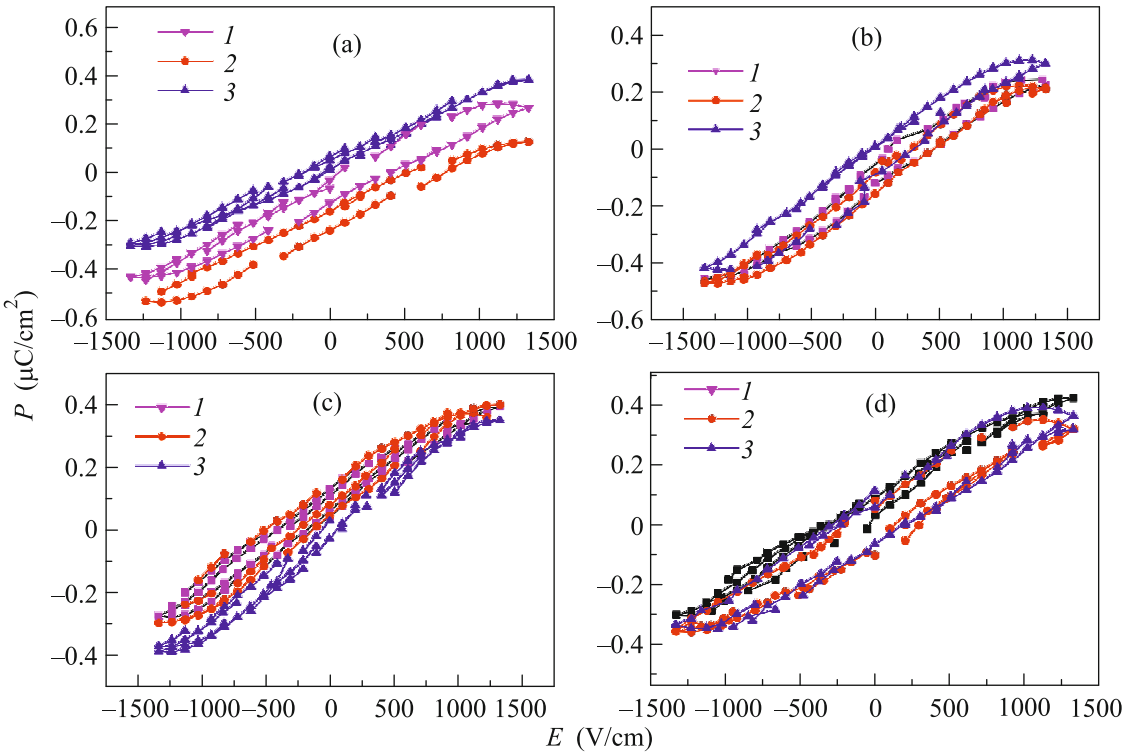

Fig. 5. (Color online) Electric polarization normal to the film deposited on the glass substrate versus the applied electric field (*1*) at zero magnetic field $H = 0$, (*2*) at the magnetic field $H^z = 12$ kOe normal to the film, and (*3*) at the magnetic field $H^x = 12$ kOe along the film at temperatures $T =$ (a) 80, (b) 160, (c) 240, and (d) 320 K.

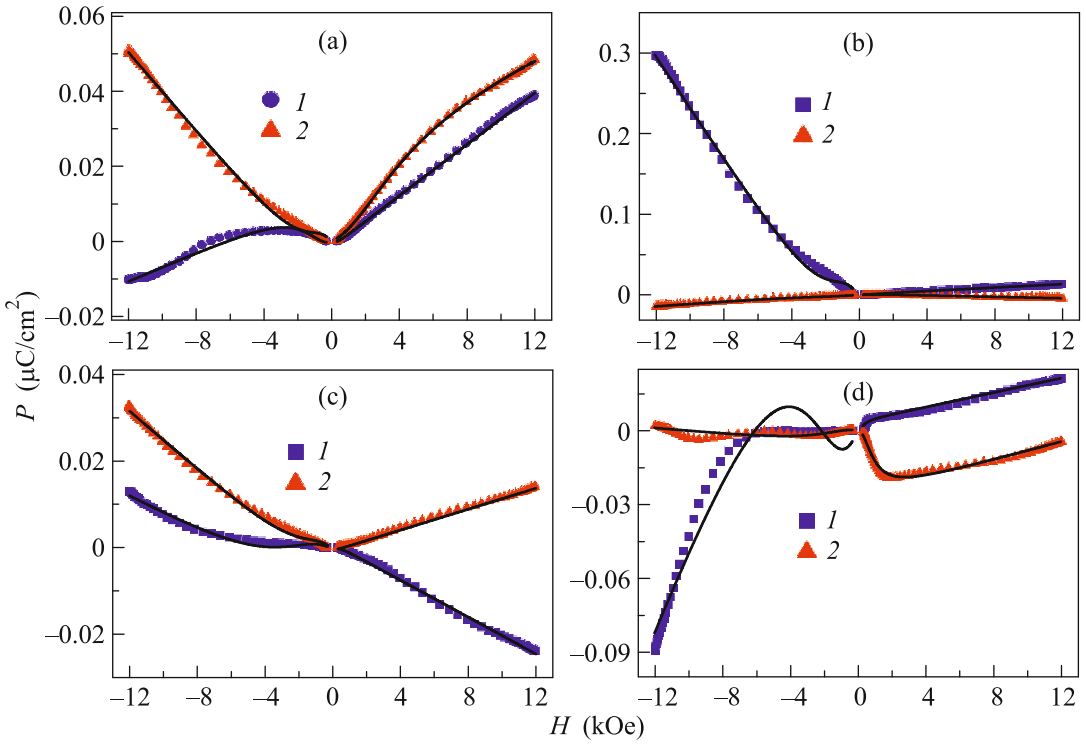

Fig. 6. (Color online) Magnetic field dependence of the electric polarization normal to the film deposited on the GGG substrate at temperatures $T =$ (a) 120, (b) 240, (c) 280, and (d) 360 K. The magnetic field is (*1*) perpendicular and (*2*) parallel to the film. The solid line corresponds to the calculations by Eq. (5).

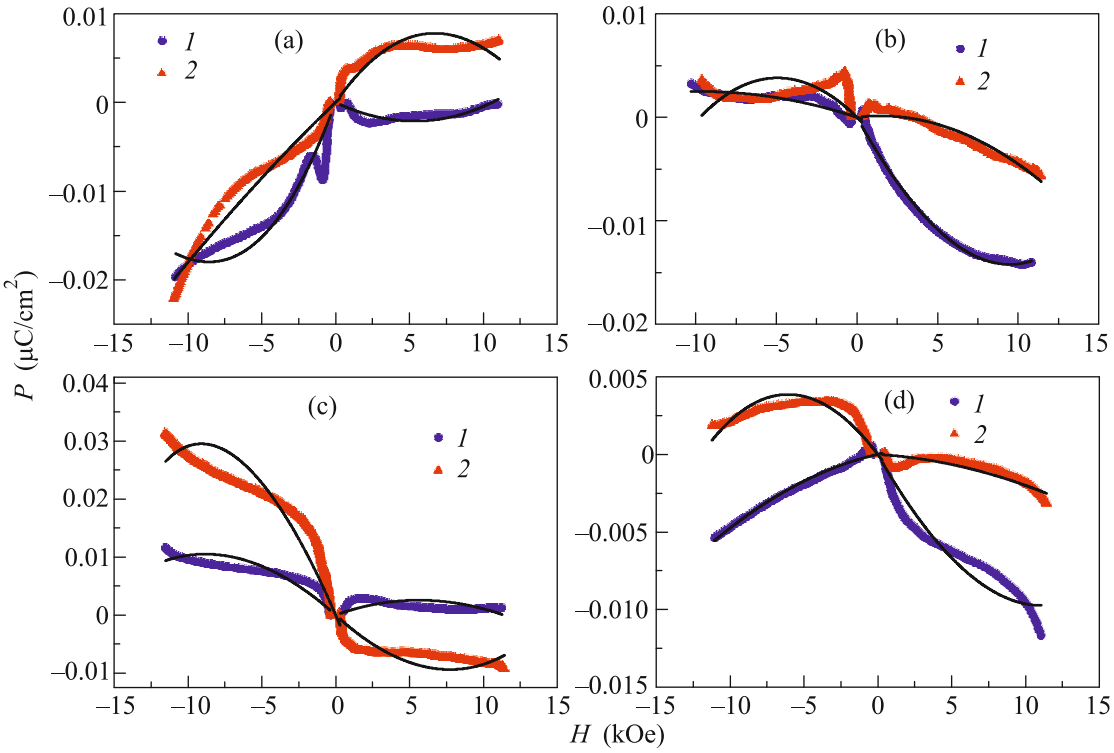

Fig. 7. (Color online) Magnetic field dependence of the electric polarization normal to the film deposited on the glass substrate at temperatures T = (a) 80, (b) 160, (c) 280, and (d) 330 K. The magnetic field is (*1*) perpendicular and (*2*) parallel to the film. The solid line corresponds to the calculations by Eq. (5).

exchanges, respectively. In the molecular field approximation, the ME tensor has the form [29]

$$\alpha_{me} = \frac{\chi_e\left(\beta_1 H + 12J\beta_2\left(1+\left(\frac{\langle S^z\rangle}{\langle S^x\rangle}\right)^2\right)\right)}{3(1+2\beta_1\langle u\rangle)^2)}, \qquad (3)$$

where $\langle u\rangle$ is the average film strain in the magnetic field. The electric polarization induced by the lattice strain in the magnetic field is fitted by the function

$$P = \frac{\gamma H^2}{1+dH^2}, \qquad (4)$$

where γ and d are the fitting parameters. The magnetic-field-induced electric polarization of the film is described by the sum of the linear and quadratic ME couplings in the magnetic field:

$$P_i = \alpha_{ij}H_j + \frac{\gamma_{ij}H_j^2}{1+dH_j^2}. \qquad (5)$$

Function (5) provides a quite satisfactory description of experimental data for $P(H)$. For the off-diagonal component of the ME tensor for the film deposited on the glass substrate, the linear contribution is dominant and $\alpha_{zx} > 0$ up to 120 K and $\alpha_{zx} < 0$ above 120 K. Up to 280 K, the diagonal component of the ME tensor is mainly determined by the linear contribution, whereas above 300 K, the quadratic ME effect with $\gamma_{ij} < 0$ is dominant. The change in the main contribution to the ME coupling and the sign reversal for the magnetostriction constant occur at the same temperature. The microscopic mechanism of the coupling between the magnetization and electric polarization involves the lattice and is related to the magnetoelastic interaction. Thin $Bi_3Fe_5O_{12}$ films deposited on the GGG substrate exhibit the sign reversal for the magneto-optical absorption at T = 300 K. In the film on the GGG substrate, the main contribution to the ME coupling for the off-diagonal tensor component comes from the quadratic ME effect, whereas the linear contribution prevails for the diagonal component.

5. CONCLUSIONS

Near the film–substrate interface, the electric polarization is induced by the bound charge in the garnet substrate. The relaxation of this polarization is described by an exponential time dependence. For the film deposited on the glass substrate, the time dependence of the relaxation of the electric polarization is described by a power law. The sign reversal for the residual polarization in the film on the glass substrate occurs after switching off the electric field. An increase in the relaxation time and a shift of the hys-

teresis loop in the applied magnetic field have been revealed. The magnetoelectric coupling depends on the characteristics of the interface, and the ME coupling for the garnet substrate is stronger than that for the glass substrate. The electric polarization of the bismuth iron garnet films is due to the bilinear EH and quadratic EH^2 effects. This is confirmed by the linear electric field ME effect. The linear response of the ME susceptibility is well interpreted within the model involving the spin–orbit coupling, whereas the quadratic ME effect results from the exchange–striction mechanism.

FUNDING

This work was supported jointly by the Russian Foundation for Basic Research, the Government of the Krasnoyarsk Territory, and the Krasnoyarsk Science Foundation (project no. 18-42-240001 "Temperature-Induced Reversal of the Sign of Magnetoelectric Tensor Components in Neodymium-Doped Bismuth Iron Garnet"), as well as in part by the Russian Foundation for Basic Research (project nos. 18-32-00079_mol_a and 18-52-00009_bel_a) and by the Russian Ministry of Science and Higher Education (state contract no. 3.5743.2017/6.7).

REFERENCES

1. T. Ishibashi, A. Mizusama, M. Nagai, S. Shimizu, K. Sato, N. Togashi, T. Mogi, M. Houchido, H. Sano, and K. Kuriyama, J. Appl. Phys. **97**, 013516 (2005).
2. E. Popova, L. Magdenko, H. Niedoba, M. Deb, B. Dagens, B. Berini, M. Vanwolleghem, C. Vilar, F. Gendron, A. Fouchet, J. Scola, Y. Dumont, M. Guyot, and N. Keller, J. Appl. Phys. **112**, 093910 (2012).
3. N. E. Khokhlov, A. E. Khramova, E. P. Nikolaeva, T. B. Kosykh, A. V. Nikolaev, A. K. Zvezdin, A. P. Pyatakov, and V. I. Belotelov, Sci. Rep. **7**, 264 (2017).
4. E. Kita, S. Takano, A. Tasaki, K. Siratori, K. Kohn, and S. Kimura, J. Appl. Phys. **64**, 5659 (1988).
5. M. Mercier, Int. J. Magn. **6**, 77 (1974).
6. D. P. Kulikova, A. P. Pyatakov, E. P. Nikolaeva, A. S. Sergeev, T. B. Kosykh, Z. A. Pyatakova, A. V. Nikolaev, and A. K. Zvezdin, JETP Lett. **104**, 197 (2016).
7. D. P. Kulikova, T. T. Gareev, E. P. Nikolaeva, T. B. Kosykh, A. V. Nikolaev, Z. A. Pyatakova, A. K. Zvezdin, and A. P. Pyatakov, Phys. Status Solidi RRL **12**, 1800066 (2018).
8. A. S. Logginov, G. A. Meshkov, A. V. Nikolaev, and A. P. Pyatakov, JETP Lett. **86**, 115 (2007).
9. A. P. Pyatakov, D. A. Sechin, A. S. Sergeev, A. V. Nikolaev, E. P. Nikolaeva, A. S. Logginov, and A. K. Zvezdin, Eur. Phys. Lett. **93**, 17001 (2011).
10. A. S. Sergeev, J. Phys.: Conf. Ser. **929**, 012085 (2017).
11. A. F. Kabychenkov, F. V. Lisovskii, and E. G. Mansvetova, JETP Lett. **97**, 265 (2013).
12. G. V. Arzamastseva, A. M. Balbashov, F. V. Lisovskii, E. G. Mansvetova, A. G. Temiryazev, and M. P. Temiryazeva, J. Exp. Theor. Phys. **120**, 687 (2015).
13. B. B. Krichevtsov, V. V. Pavlov, and R. V. Pisarev, JETP Lett. **49**, 535 (1989).
14. E. Popova, A. Shengelaya, D. Daraselia, D. Japaridze, S. Cherifi-Hertel, L. Bocher, A. Gloter, O. Stephan, Y. Dumont, and N. Keller, Appl. Phys. Lett. **110**, 142404 (2017).
15. T. Oikawa, S. Suzuki, and K. Nakao, J. Phys. Soc. Jpn. **74**, 401 (2005).
16. S. Wittekoek, T. J. A. Popma, J. M. Robertson, and P. F. Bongers, Phys. Rev. B **12**, 2777 (1975).
17. Y. Hosoe, R. Suzuki, K. Takanashi, H. Yasuoka, S. Chikazumi, and Y. Sugita, J. Phys. Soc. Jpn. **55**, 731 (1986).
18. M. M. Parish, Nature (London, U.K.) **426**, 162 (2003).
19. A. M. Essin, A. M. Turner, J. E. Moore, and D. Vanderbilt, Phys. Rev. B **81**, 205104 (2010).
20. A. Malashevich, I. Souza, S. Coh, and D. Vanderbilt, New J. Phys. **12**, 053032 (2010).
21. M. Sasaki, G. Lou, Q. Liu, M. Ninomiya, T. Kato, S. Iwata, and T. Ishibashi, Jpn. J. Appl. Phys. **55**, 055501 (2016).
22. S. S. Aplesnin, A. N. Masyugin, M. N. Sitnicov, U. I. Rybina, and T. Ishibashi, J. Magn. Magn. Mater. **464**, 44 (2018).
23. T. Ishibashia, A. Mizusawa, M. Nagai, S. Shimizu, and K. Satoet, J. Appl. Phys. **97**, 013516 (2005).
24. A. K. Zvezdin and A. P. Pyatakov, Phys. Usp. **52**, 845 (2009).
25. J. van den Brink and D. I. Khomskii, J. Phys.: Condens. Matter **20**, 434217 (2008).
26. I. A. Sergienko and E. Dagotto, Phys. Rev. B **73**, 094434 (2006).
27. M. A. Essin, A. M. Turner, J. E. Moore, and D. Vanderbilt, Phys. Rev. B **81**, 205104 (2010).
28. A. Scaramucci, E. Bousquet, M. Fechner, M. Mostovoy, and N. A. Spaldin, Phys. Rev. Lett. **109**, 19 (2012).
29. V. V. Shvartsman, P. Borisov, W. Kleemann, S. Kamba, and T. Katsufuji, Phys. Rev. B **81**, 064426 (2010).

Translated by K. Kugel